ANALYSIS OF SIR-A ANTENNA TESTS

Final Report

by

Keith R. Carver

Cecil C. Post

prepared for

NASA Johnson Space Center

Houston, Texas

Contract No.

NAS 9-95482

January 1979

NEW MEXICO STATE UNIVERSITY

Physical Science Laboratory

BOX 3-PSL, LAS CRUCES, NEW MEXICO 88003

AREA (505) 522-4400 TWX 910-983-0541

TABLE OF CONTENTS

1.0 INTRODUCTION

The purpose of this report is (1) to provide an analysis of antenna test procedures used at JPL for measurement of the SIR-A antenna and (2) to point out that the measured E-plane patterns differ in some significant respects from the true pattern as experienced during the OFT-2 space deployment; this results principally from the finite range length associated with the JPL far-field range.

The SIR-A antenna is a microstrip patch planar array which is 9.38m x 2.09m in size and is manufactured by Ball Brothers Research Corporation (BBRC). The antenna is being procured by NASA Johnson Space Center (JSC) for use in the JPL-designed SIR-A experiment to go on the Shuttle OFT-2 mission and was tested at the JPL West Mesa Antenna Range during the period October-December, 1978. PSL has provided advisory support to NASA/JSC during this SIR-A test phase by monitoring tests at JPL and by careful analysis of both the test data and the most probable antenna pattern performance to be obtained under OFT-2 deployment conditions.

2.0 ANALYSIS OF THE JPL ANTENNA TEST PROCEDURES

2.1 Mechanical

There was good coordination between Ball Brothers Research Corporation (BBRC) and the Jet Propulsion Laboratory (JPL) cognizant personnel in both the preparation for and in the mechanical handling of the SIR-A antenna. The JPL procedures outline described in detail how each step in the handling process should be carried out. Storage during off-work periods was well planned, and off-hour monitoring of the storage area humidity and temperature was automatically recorded and manually observed. The antenna range mount worked well; it was stable, and positions were repeatable.

The mechanical boresighting of the SIR-A antenna and the range mount procedures were well done be JPL personnel. The mirror image described a 3 inch circle around the roll axis as the SIR-A antenna was rolled through 360 degrees. The boresight range was 150 feet giving an optical equivalent path length of 300 feet; this represents a ± .025° error about the roll axis. This is a fixed systematic error. In budgets for the beam pointing error, the experimental error must be added to this. Since the observed repeatability was .092°, these two numbers may be combined to provide a lower bound for the most probable error:

$$\varepsilon = \sqrt{(.05)^2 + (.092)^2} = \pm\ .105° \qquad (2.1)$$

2.2 Electrical

2.2.1 Beam Pointing

Beam pointing was measured separately for the E-plane and the H-plane by observing the angles read at the -3dB points on either side of the peak signal with a theodolite and a target of opportunity. This method was questioned at the beginning but all observers finally agreed that the beam direction was known correctly. A tilt in the E-plane toward $\phi = 180°$ of $\theta = 0.0683°$ and a tilt in the H-plane toward $\phi = 90°$ of $\theta = 0.0608°$ was measured. Using a distance of 3136 feet to the source provides a beam pointing direction of $(\theta, \phi) = (0.091°, 138.3°)$.

2.2.2 Gain

The gain of three standard antennas was first determined by the three antenna method utilizing a deMornay-Bonardi model dB-300 insertion loss measuring device, and a known range distance. Measurements gave the following gains at 1278 MHz.

PSL Standard Gain Horn = +15.60 dBi
JPL Standard Gain Horn = +15.68 dBi
JPL Panel (Modified BBRC Panel) = +23.08 dBi

The JPL panel was used for comparison with the SIR-A antenna. No error has been stated by JPL for this measurement as of this writing.

The SIR-A antenna gain may be estimated from measured antenna 3-dB beamwidths, which are:

6° (H-plane)
1.28° (E-plane)

This well-known directivity formula, which is applicable to low sidelobe antennas, is [1]:

$$D = \frac{41,253}{6^\circ \times 1.28^\circ} = 37.30 \text{ dB} \qquad (2.2)$$

The antenna efficiency of a single panel was determined by BBRC to be 51%. Thus assuming that the same efficiency holds for SIR-A:

$$.51D = +34.38 \text{ dB} \qquad (2.3)$$

The estimated line loss is -0.6 dB so that the predicted gain is G = 33.8 dBi. The measured gain (an average of three measurements) was 33.62 dBi.

2.2.3 Gain Error

All the error factors involved in the gain are not known at PSL, but as a minimum the following should be considered:

Range reflections SG-Panel probe = ± .065 dB
Range reflections SIR-A probe = ± .03 dB
Experimental spread SIR-A gain = ± .072 dB

2.2.4 Comments

The JPL antenna range is very well equipped with an adequate staff for data recording and mechanical handling. Careful efforts were made throughout the measurement period to provide JSC and BBRC with reliable and repeatable data. However, despite these strengths, the JPL antenna range facility does not seem to have adequate staffing for detailed analyses of range performance, error budgets, etc. It appeared that virtually the entire burden of JPL test planning and coordination, as well as range and data analysis was placed on the shoulders of one JPL engineer; this is too great a load for one person. As a result, JPL seemed particularly weak in the areas of understanding the significance of range reflections, the detailed analysis of such range characteristics as finite path length effects on sidelobe levels and phase patterns, detailed error budgets, etc. This is not intended as a criticism of the JPL antenna engineer, but is meant to convey the need for more JPL analytical support in the area of antenna metrology.

In addition to this comment, there are additional observations which may be helpful in improving future measurement programs.

1. There was initially some confusion in proper methods for identifying the cross-polarized patterns in relation to the principal component patterns.

2. A complete error analysis should be provided by JPL to JSC, detailing both systematic and random errors.

3. An analysis of the effects of range reflections should be included in the above.

4. An analysis should be provided by JPL of methods used to measure antenna patterns as applied to power contour graphs. The JPL method, as observed by PSL personnel, was to normalize the recorder to a particular power level for each roll cut. This was done because a 0.5 dB power drift was observed for a 3 time period of 4.7 minutes. This normalizing procedure is questionable if the data is used to produce a power contour plot. It may be necessary to include the 0.5 dB drift in the error analysis.

3.0 SIR-A PATTERNS: MEASURED vs. TRUE

Although several analyses of the SIR-A antenna patterns have previously been carried out by both PSL and BBRC [2, 3, 4, 5, 6], none of these has adequately addressed the effect of the finite range length (3136') of the JPL West Mesa Antenna Range, while at the same time incorporating the effects of the true aperture amplitude and phase distribution. This section will show that (a) the mathematical model and numerical results presented herein agree well with the measured far-field amplitude and phase patterns, and (b) the finite range length (3136') produces a measured pattern which is different from the true in-situ pattern (as deployed on the Shuttle) in two important regards: (1) the measured E-plane phase vs. angle pattern is almost entirely a result of the finite antenna range length, and (2) pattern amplitude nulls are much deeper than appears from measured data to be the case.

3.1 Antenna Pattern Analysis: Aperture Distribution

At the JPL 3136' range, the wave incident on the SIR-A antenna is not truly a plane wave; it is a spherical wave with a 3136' radius of curvature, as shown in Figure 3.1. This means that the antenna is not being tested under true plane-wave-incidence conditions, and that effectively the phase of the edge lags that of the center by an amount

$$\Delta = \frac{2\pi\ell}{\lambda} \text{ (radians)} \tag{3.1}$$

where

$$\ell = \sqrt{(3136)^2 + (L/2)^2} - 3136 \quad \text{(ft.)} \tag{3.2}$$

For the SIR-A E-plane, $L/2 \cong 16'$ so that

$$\ell = .0408' \quad (1.2435 \text{ cm}), \tag{3.3}$$

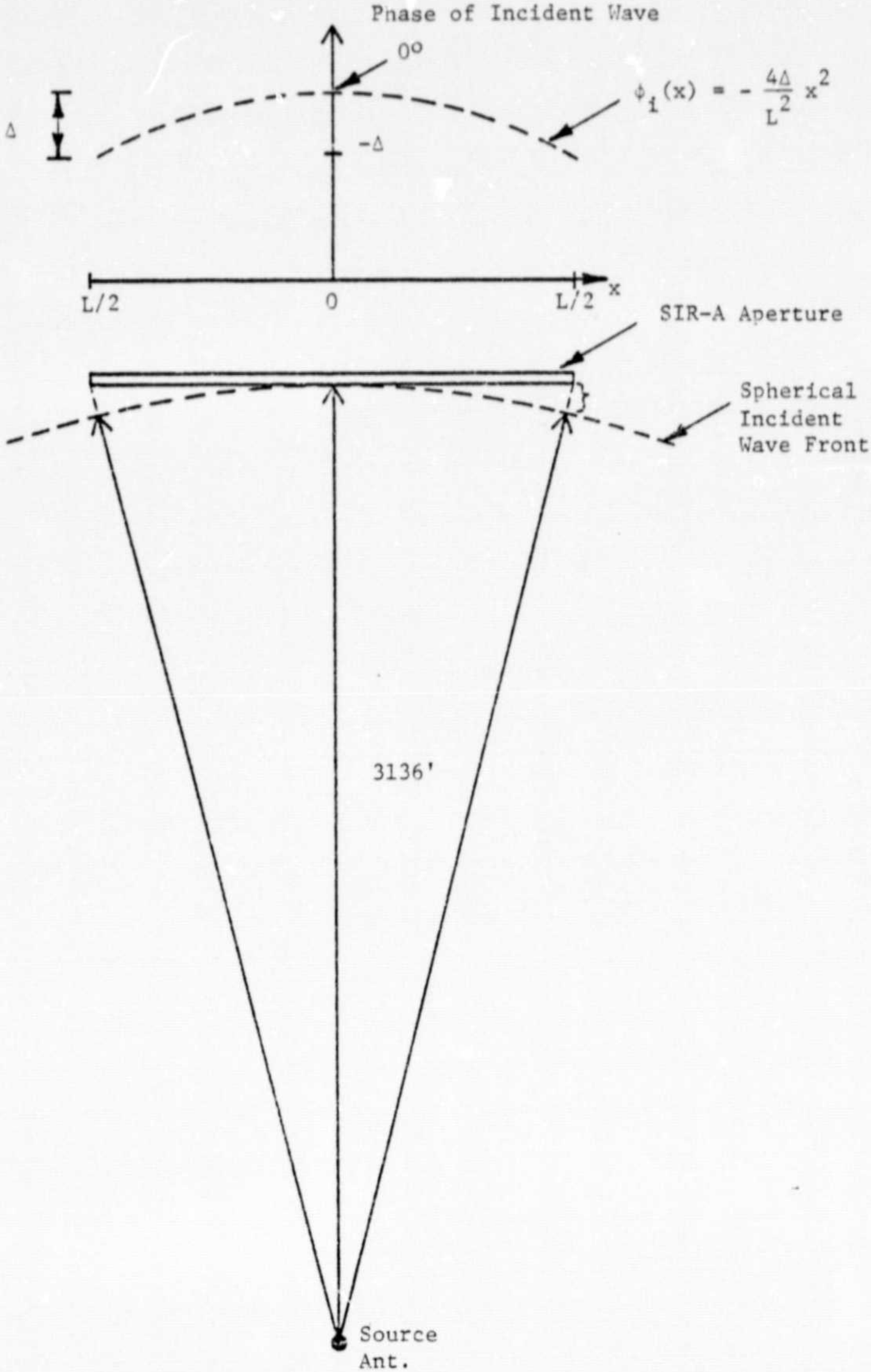

Figure 3.1 Illustrating finite range length effect on phase distribution of incident wave (not to scale)

so that at 1278 MHz (λ = 23.474 cm),

$$\Delta = .333 \text{ rad} \quad (19.1°) \tag{3.4}$$

To a very good approximation, the phase of the incident wave may be written as a parabolic contour

$$\phi_i(x) = -\alpha x^2 \tag{3.5}$$

where

$$\alpha = \frac{4\Delta}{L^2} \tag{3.6}$$

and

$$x = \text{distance along aperture, measured from center}$$

The standard diffraction integral for the far-zone electric field of an aperture is

$$E(\theta) = \cos\theta \int_{-L/2}^{L/2} I(x)\, e^{jkx \sin\theta}\, dx \tag{3.7}$$

where θ is the angle measured from broadside and $I(x)$ is the aperture current distribution. Although the SIR-A BBRC antenna is actually an array, there is a sufficient number of elements so that the aperture distribution $I(x)$ may be represented as a piecewise continuous function. It is further assumed that each of the seven panels has a uniform current and a uniform phase, but that these values are different for each panel. The current amplitude of each panel is determined by:

1. The feedline network nominal design

2. Individual values of the reflection coefficient at the input to each panel

3. Panel manufacturing tolerances (as measured by changes in the peak gain for each panel)

Unfortunately, only the magnitude of the input reflection coefficients for each panel is known by PSL; these are based on BBRC-measured values of the VSWR [2]. Calculations herein have been based on worst-case assumed values of the reflection coefficient phases. The nominal design of the feed network delivers a relative power of 1/8 to the four outside panels (two on each end) and 1/6 to the center three panels. Finally, differences in current amplitude due to panel manufacturing tolerances can be observed by noting the change in individual panel gains [2]. These factors are summarized in Table 3.1.

Table 3.1

SIR-A E-Plane Current Amplitude Factors

Panel Position	Feed Network Nominal Design (Power)	(Current)	Individual Refl. Coeff. Ampl. (VSWR)	$\lvert\rho\rvert$	Individual Gains (dB)	(Current)
		F_N				F_G
1	1/8	0.866	1.16	.074	25.93dBi	.9661
2	1/8	0.866	1.14	.064	25.86	.9583
3	1/6	1.000	1.12	.057	26.03	.9772
4	1/6	1.000	1.12	.057	26.13	.9886
5	1/6	1.000	1.06	.029	26.23	1.000
6	1/8	0.866	1.17	.078	25.87	.9594
7	1/8	0.866	1.14	.064	26.10	.9851

The relative current amplitude for each panel may be computed as

$$I_m = F_N F_G \tag{3.8}$$

where

F_N = relative current produced by a perfect feed network and identical matched panels

F_T = transmission coefficient from feedline to mth panel

$$= |1 + \rho| = \left|1 + |\rho_m| e^{j\phi_n}\right| \qquad (3.9)$$

$(F_T)_{max} = 1 + |\rho_m|$; $(F_T)_{min} = 1 - |\rho_m|$

F_G = relative tolerance-caused change in current (w.r.t. 1.0) as evidenced by measured gains of individual panels w.r.t. panel #5.

Of course, the individual gain factor F_G is influenced in part by the input reflection coefficient factor F_R; however, F_G is also influenced by the antenna efficiency k_L ($0 \leq k_L < 1$) which is dependent only on the internal heating losses. Thus, the peak gain of panel m (relative to panel 5) would be given by

$$F_G^{(m)} = \frac{F_T^{(m)} \; k_L^{(m)}}{F_T^{(5)} \; k_L^{(5)}} \qquad (3.10)$$

Assuming that the heat-loss factor is identical for each panel, i.e. $k_L^{(m)} = k_L^{(5)}$,

$$F_G^{(m)} = \frac{|1 + \rho_m|}{|1 + \rho_s|} \qquad (3.11)$$

If it is assumed that $\rho_m = -|\rho_m|$, it will be seen that the predicted values of relative gain from (3.11) agree well with the BBRC-measured values from Table 3.1. This strongly suggests that variations in gain of the individaul panels derive mostly from individual mismatch differences.

Using equation (3.8) and appropriate values from Table 3.1, the relative panel currents can be computed and listed, as in Table 3.2.

Table 3.2
Computed Relative Currents
for SIR-A Panels

Panel Position	Relative Current
1	0.8367
2	0.8299
3	0.9772
4	0.9886
5	1.000
6	.8308
7	.8531

The phase of the current across each panel is determined by two parameters:

1. The insertion phase S_m of each panel. This has been measured by BBRC [7] and is listed in Table 3.3.

2. The quadratic phase taper $\phi_i(x)$ due to the finite range length, as shown in Figure 3.1 and calculable from Equation (3.5).

Table 3.3
Measured Insertion Phases
of SIR-A Panels

Panel Position	Insertion Phase, S_m
	(deg.)
1	+ 2°
2	- 12°
3	- 14°
4	0°
5	+ 4°
6	+ 3°
7	+ 4°

3.2 Antenna Pattern Analysis: Far-Field Patterns

If the total E-plane array length is L, then each of the seven panels has a length L/7. The total field is then given by

$$E(\theta) = \cos\theta \sum_{m=1}^{7} E_m(\theta) \tag{3.12}$$

where, from (3.7),

$$E_m(\theta) = I_m e^{j\delta_m} \int_{x_m-L/14}^{x_m+L/14} e^{-j\alpha x^2} e^{jkx \sin\theta} dx \tag{3.13}$$

and where

$$\delta_m = (m-4)\frac{L}{7} \quad (m = 1,2,\ldots,7)$$

$$k = 2\pi/\lambda$$

$$\alpha = \frac{4\Delta}{L^2}$$

The integral of (3.13) can be rewritten as a Fresnel integral; however, since α is small, the quadratic phase term can be expanded in the first two terms of a binomial series, i.e.,

$$e^{-j\alpha x^2} \cong 1 - j\alpha x^2 + \ldots \tag{3.14}$$

Thus,

$$E_m(\theta) = I_m e^{j\delta_m} \left\{ \int_{x_m - \frac{L}{14}}^{x_m + \frac{L}{14}} e^{jkx \sin\theta} \, dx - j\alpha \int_{x_m - \frac{L}{14}}^{x_m + \frac{L}{14}} x^2 e^{jkx \sin\theta} \, dx \right\} \quad (3.15)$$

These are standard integrals and the evaluation is straightforward although details are messy. The resulting E-plane field pattern (normalized to 1 for an infinite range length and $\delta_m = 0$ for all m) is

$$E(\theta) = \frac{\cos\theta}{7} \sum_{m=1}^{7} I_m e^{j\delta_m} e^{2j(m-4)X} \left\{ \frac{\sin X}{X} + \frac{\Delta}{49} (a_m - jb_m) \right\} \quad (3.16)$$

where

$$X = \frac{kL}{14} \sin\theta \quad (3.17)$$

$$a_m = \frac{4(m-4)}{X} \left\{ \frac{\sin X}{X} - \cos X \right\} \quad (3.18)$$

$$b_m = [4(m-4)^2 + 1] \frac{\sin X}{X} - \frac{2}{X^2} \left[\frac{\sin X}{X} - \cos X \right] \quad (3.19)$$

The second term in the braces of Equation (3.16) is due to the quadratic phase error associated with the finite range length of the JPL range. For this range, $\Delta = .333$ rad. However, as the SIR-A antenna is deployed on the shuttle, the range is essentially infinite so that $\Delta = 0$, leaving only the array factor for a seven-element array of $\frac{L}{7}$ - length panels with individual amplitudes (I_m) and phases (δ_m).

3.3 SIR-A Pattern: Numerical Results

Figures 3.2 and 3.3 illustrate antenna amplitude and phase pattern comparisions between JPL-measured data [8] and calculations based on the preceding theory. The numerical values were obtained from a computer program [see Appendix] written for a TI-59 programmable calculator; for the SIR-A E-plane, kL = 251. The agreement is very good, except for the second null position to the left and the first null depth and position to the right. It will be recalled from preceding analysis that with an approximate JPL range reflectivity of -21 dB, the uncertainty in the measured value of the power pattern can be several dB at the -25 dB to -30 dB level, depending on the exact angle(s) at which the interfering reflected signal enters the pattern. Thus, there is no compelling reason to assert that the measured E-plane patterns inspire significantly more confidence than the calculated patterns presented here; this is particularly true for the phase patterns.

The calculated patterns show a beam tilt to the right of 0.060°; the measured value was .061° ± .034°. The calculated -8 dB E-plane beamwidth is 2.009°; the measured value was 1.988° ± .002°. The calculated E-plane sidelobe levels are (-12.7 dB, $-\theta$; -17.8dB, $+\theta$); the measured levels were (-12.2 dB; -17.8 dB). All of these comparisons illustrate that the significant features of the pattern shape can be very accurately obtained from the theoretical model presented herein when supplemented by a knowledge of individual panel gains and insertion phases, and considering the finite range length effect.

The true deployment pattern of the SIR-A antenna can thus be accurately obtained by a calculated pattern based on Equation (3.16) and letting the range be that of the shuttle-to-earth distance, i.e. $\Delta \cong 0$.

The resulting amplitude and phase patterns thus obtained are shown in Figures 3.4 and 3.5, where a comparison is made between the calculated patterns for the JPL range and the calculated patterns for OFT-2 deployment conditions, i.e., $\Delta = 0$. The most obvious effects in the power pattern are that (1) the nulls are much sharper and (2) the sidelobe levels are slightly reduced below those predicted for JPL range test conditions. The OFT-2 deployment pattern has a much flatter phase pattern over the -8 dB beamwidth than that predicted

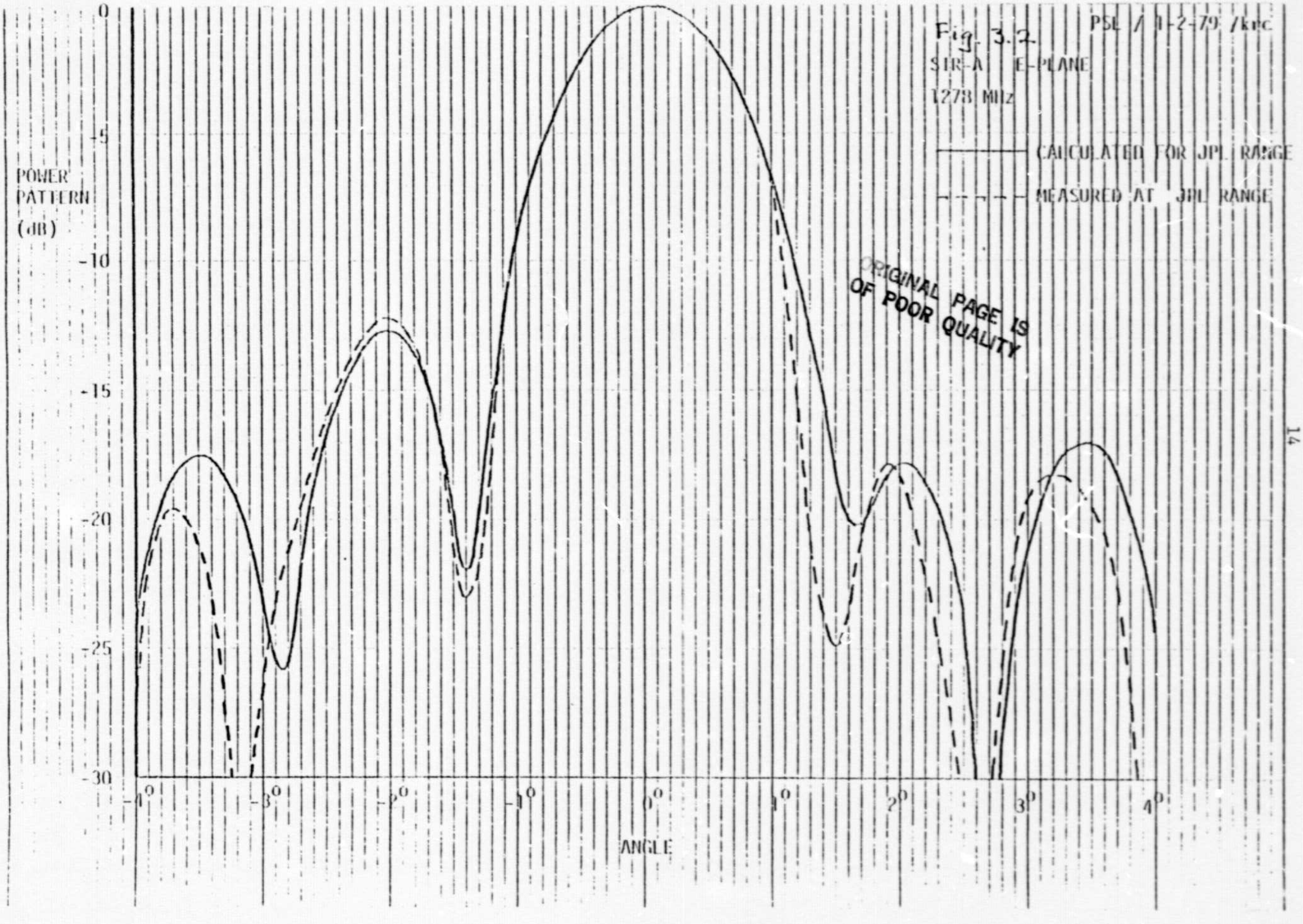
Fig. 3.2
PSL / 1-2-79 /krc
SIR-A E-PLANE
1278 MHz
CALCULATED FOR JPL RANGE
MEASURED AT JPL RANGE
POWER PATTERN (dB)
0
-5
-10
-15
-20
-25
-30
-4°
-3°
-2°
-1°
0°
1°
2°
3°
4°
ANGLE

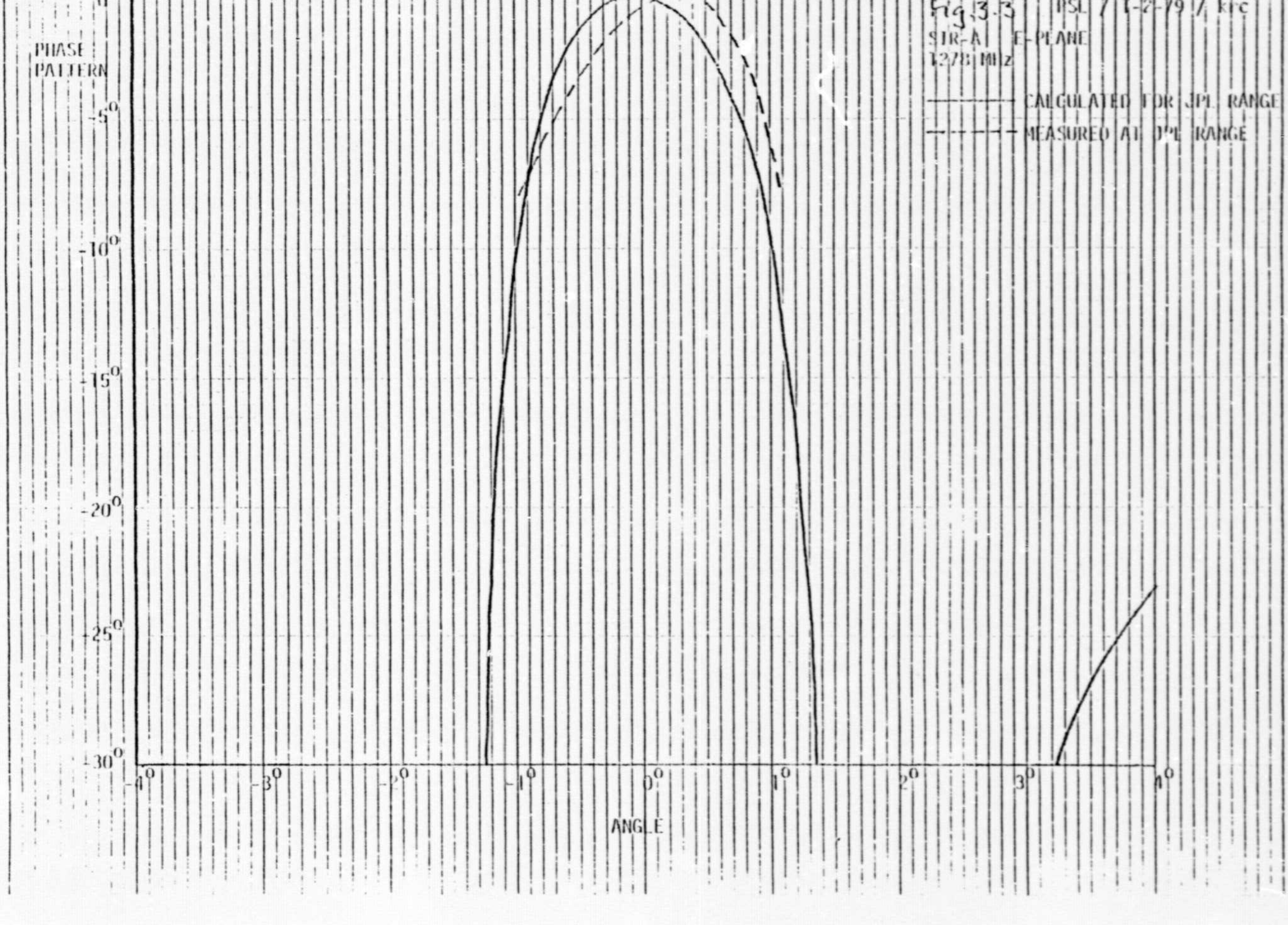
Fig. 3.3 PSL / 1-2-79 / krc
STR-A E-PLANE
1278 MHz
CALCULATED FOR JPL RANGE
MEASURED AT JPL RANGE
PHASE PATTERN
0°
-5°
-10°
-15°
-20°
-25°
-30°
-4°
-3°
-2°
-1°
0°
1°
2°
3°
4°
ANGLE

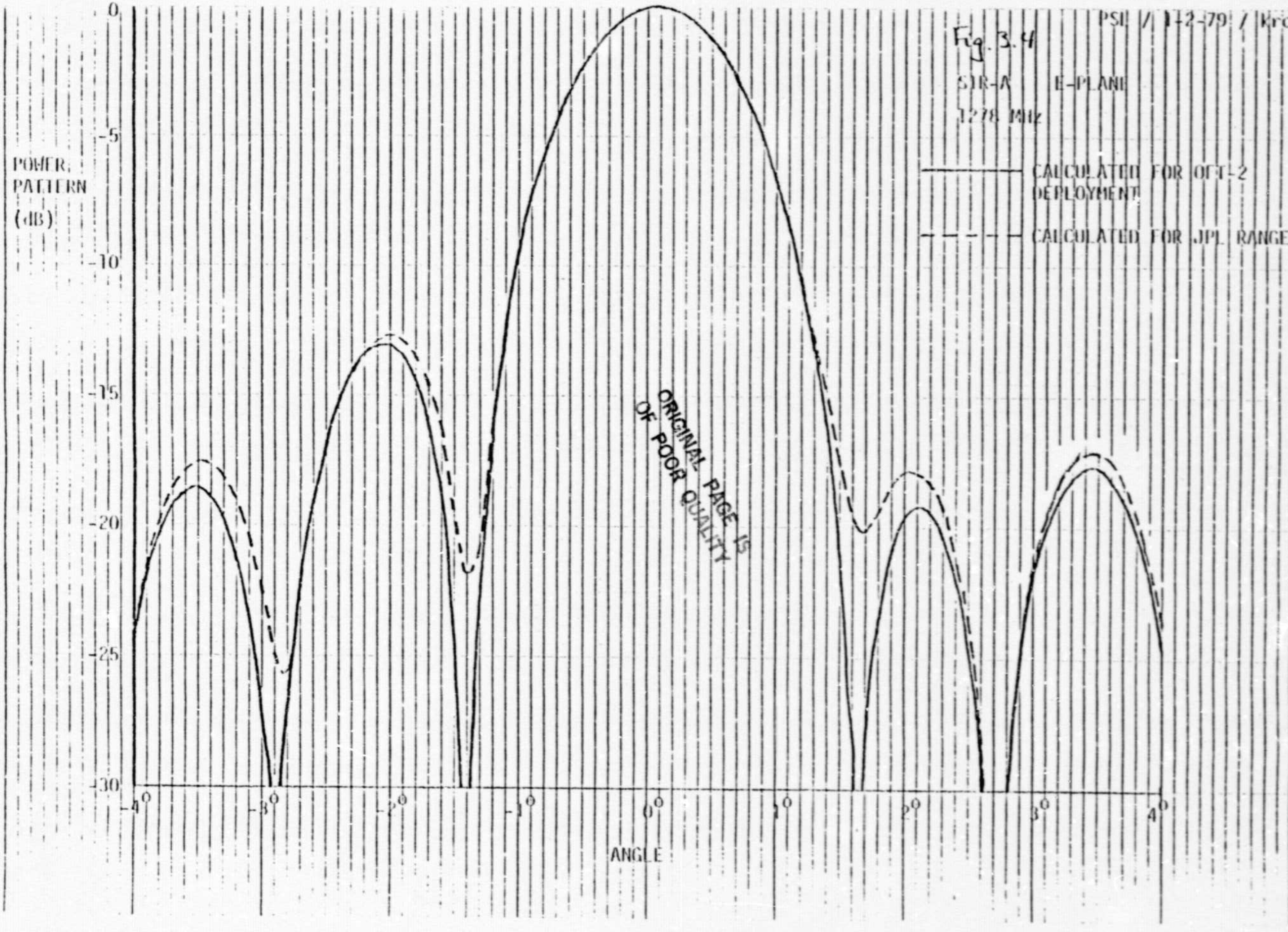
PSL / 1-2-79 / Krc
Fig. 3.4
SIR-A E-PLANE
1278 MHz
CALCULATED FOR OFT-2 DEPLOYMENT
CALCULATED FOR JPL RANGE
POWER PATTERN (dB)
0
-5
-10
-15
-20
-25
-30
-4^0
-3^0
-2^0
-1^0
0^0
1^0
2^0
3^0
4^0
ANGLE

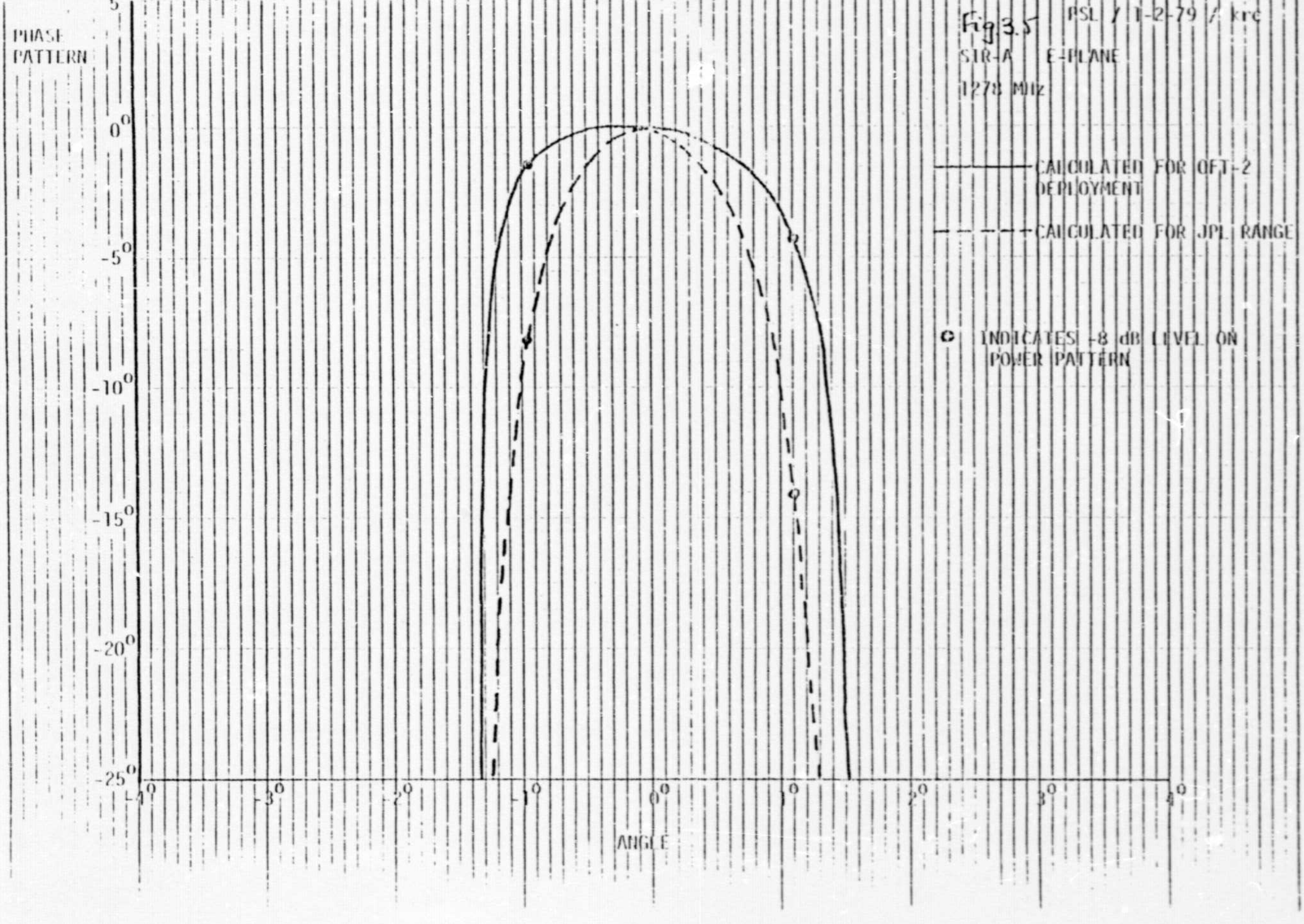
PHASE PATTERN
Fig 3.5
PSL / 1-2-79 / krc
SIR-A E-PLANE
1278 MHz
CALCULATED FOR OFT-2 DEPLOYMENT
CALCULATED FOR JPL RANGE
INDICATES -8 dB LEVEL ON POWER PATTERN
5°
0°
-5°
-10°
-15°
-20°
-25°
-4°
-3°
-2°
-1°
0°
1°
2°
3°
4°
ANGLE

for the JPL test data. This is to be expected, since much of the concave shape of the measured phase curve is due to the quadratic phase error of the illuminating wave associated with the JPL range length.

Is is strongly recommended that the E-plane phase data measured by JPL not be taken as the true phase pattern that would be experienced under deployment conditions. The calculated solid curve of Figure 3.5 is a much more accurate representation.

In order to provide an estimate of the worst-case quadratic phase error associated with this phase behavior, a 6th-degree polynomial was found which provides a best fit (in the least-squares sense) to the calculated phase curve over the angular range $\pm$ 1.2°. This curve is shown as the solid line in Figure 3.6; the actual phase values are shown as asterisks. The polynomial is given by

$$\phi = \sum_{n=0}^{6} c_n \, \theta^n \tag{3.20}$$

where

ϕ = far-field phase (deg.)
θ = angle from axis (deg.)
C_0 = .026015
C_1 = -.387169
C_2 = -2.156546
C_3 = -.937944
C_4 = 1.381933
C_5 = .714718
C_6 = -1.705156

The maximum quadratic phase error is incurred at θ = 1.08°, where the power pattern is at -8 dB; the value is 2.6° which is well within specifications.

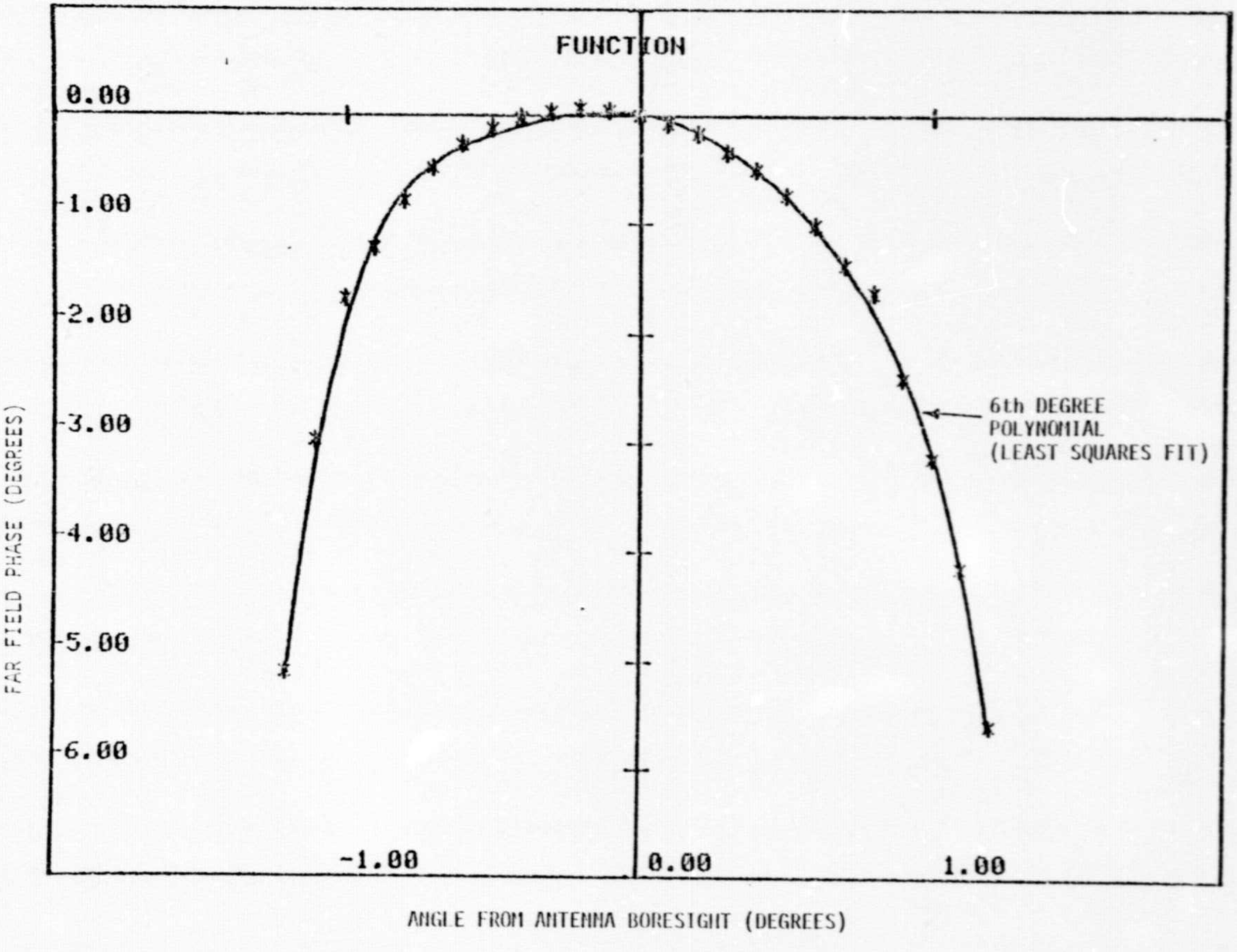
FUNCTION
0.00
-1.00
-2.00
-3.00
-4.00
-5.00
-6.00
FAR FIELD PHASE (DEGREES)
6th DEGREE
POLYNOMIAL
(LEAST SQUARES FIT)
-1.00
0.00
1.00
ANGLE FROM ANTENNA BORESIGHT (DEGREES)

4.0 CONCLUSIONS AND RECOMMENDATIONS

This report has summarized the principal highlights of the test procedure used at JPL and has also provided a detailed mathematical analysis of the SIR-A E-plane pattern. The differences between the measured and calculated E-plane patterns are slight, although the calculated E-plane patterns are considered to be more representative of the *in-situ* OFT-2 deployment patterns than are the measured patterns; this is particularly true of the SIR-A phase pattern, where it is shown from the calculated patterns that the maximum quadratic phase error (over the -8 dB beamwidth) is 2.6°.

It is recommended that the JPL-measured nominal values be used for: (1) beam tilt, (2) gain, (3) sidelobe level, (4) cross-polarization level, (5) -8 dB beamwidth, and (6) H-plane pattern amplitude and phase shape. It is recommended that the PSL-calculated values be used for the E-plane pattern amplitude and phase shape. Finally, it is recommended that JPL provide a complete error analysis for all principal measured data.

5.0 REFERENCES

1. Kraus, J. D. and K. R. Carver, "Electromagnetics," 2nd Edition, McGraw-Hill Book Co., New York, 1973.

2. Coffey, E. L. and K. R. Carver, "Antenna Evaluation Study for the Shuttle Multispectral Radar: Phase I," PSL Tech. Report No. PA00874, December 1976.

3. Coffey, E. L. and K. R. Carver, "Antenna Evaluation Study for the Shuttle Multispectral Radar: Phase II," PSL Tech. Report No. PA00881, May, 1977.

4. Coffey, E. L. and K. R. Carver, "Antenna Evaluation Study for the Shuttle Multispectral Radar: Phase III," PSL Tech. Report, January, 1979.

5. Carver, K. R., E. L. Coffey and T. F. Bush, "Review of Shuttle Imaging Radar Antenna Test and Simulation Studies," presented at NASA/JSC, January 3, 1978; PSL/NMSU briefing document.

6. Murphy, L., Section 5 in "PDR-SIR-A Antenna," Ball Brothers Research Corp., Boulder, CO, March, 1978.

7. Schoep, V. R., "SIR-A: Summary of Panel Characteristics," Ball Brothers Research Corp., System Engineering Report SIR-A-145, November 9, 1978, 3 pp.

8. Keeler, L., "Summary of SIR-A Measured Data," private communication. JPL, Pasadena, CA, December, 1978.

6.0 APPENDIX

This appendix presents a listing of the computer program used for the calculated patterns in Section 3.3 and also a listing of the numerical results. The program, based on Equations (3.16) through (3.19) with input data from Tables 3.2 and 3.3 was written using one of the author's (KRC) TI-59 programmable calculator. The data values were printed by the TI PC-100A printer as a listing of far-field amplitude and phase values associated with each angle, i.e.

$-\theta$:	1.500	(the negative of the angle in degrees)
P(dB)	-17.234	(power level in dB)
ϕ(deg.)	11.126	(phase angle in degrees)

Data points are calculated for angles between ± 4° from broadside and at increments of 0.05°.

SIR-A ANT. PROGRAM

SIR-A TI-59

```
Enter I1     000  76  LBL
             001  23  LNX
             002  42  STO
             003  30   30
             004  99  PRT
             005  91  R/S
Enter I2     006  76  LBL
             007  24  CE
             008  42  STO
             009  31   31
             010  99  PRT
             011  91  R/S
Enter I3     012  76  LBL
             013  32  X:T
             014  42  STO
             015  32   32
             016  99  PRT
             017  91  R/S
Enter I4     018  76  LBL
             019  33  X²
             020  42  STO
             021  33   33
             022  99  PRT
             023  91  R/S
Enter I5     024  76  LBL
             025  34  √X
             026  42  STO
             027  34   34
             028  99  PRT
             029  91  R/S
Enter I6     030  76  LBL
             031  35  1/X
             032  42  STO
             033  35   35
             034  99  PRT
             035  91  R/S
Enter I7     036  76  LBL
             037  67  EQ
             038  42  STO
             039  36   36
             040  99  PRT
             041  91  R/S
Enter δ1     042  76  LBL
             043  28  LOG
             044  42  STO
             045  37   37
             046  99  PRT
             047  91  R/S
Enter δ2     048  76  LBL
             049  29  CP
             050  42  STO
             051  38   38
             052  99  PRT
             053  91  R/S
Enter δ3     054  76  LBL
             055  37  P/R
             056  42  STO
             057  39   39
             058  99  PRT
             059  91  R/S
Enter δ4     060  76  LBL
             061  38  SIN
             062  42  STO
             063  40   40
             064  99  PRT
             065  91  R/S
Enter δ5     066  76  LBL
             067  39  COS
             068  42  STO
             069  41   41
             070  99  PRT
             071  91  R/S
Enter δ6     072  76  LBL
             073  30  TAN
             074  42  STO
             075  42   42
             076  99  PRT
             077  91  R/S
Enter δ7     078  76  LBL
             079  79  x̄
             080  42  STO
             081  43   43
             082  99  PRT
             083  91  R/S
Enter Δ      084  76  LBL
             085  11   A
             086  42  STO
             087  01   01
             088  99  PRT
             089  91  R/S
Enter kL     090  76  LBL
             091  12   B
             092  42  STO
             093  02   02
             094  99  PRT
             095  91  R/S
Angle θ      096  76  LBL
             097  13   C
             098  55   ÷
             099  05   5
             100  07   7
             101  93   .
             102  02   2
             103  09   9
             104  05   5
             105  07   7
             106  08   8
             107  95   =
             108  42  STO  ] θ
             109  03   03 ] (rad)
             110  38  SIN
             111  65   ×
             112  43  RCL
             113  02   02
             114  55   ÷
             115  01   1
             116  04   4
             117  95   =
             118  42  STO  ] X
             119  04   04 ]
             120  38  SIN
             121  55   ÷
             122  43  RCL
             123  04   04
             124  95   =
             125  42  STO  ] sin X / X
             126  05   05 ]
             127  43  RCL
             128  04   04
             129  39  COS
             130  55   ÷
             131  43  RCL
             132  04   04
             133  95   =
             134  42  STO  ] cos X / X
             135  06   06 ]
---------------------------------
             136  71  SBR
             137  88  DMS
---------------------------------
             138  07   7
             139  42  STO  m=7
             140  00   00
---------------------------------
Begin sum    141  76  LBL
             142  14   D
             143  53   (
             144  04   4
             145  65   ×
             146  53   (
             147  43  RCL
             148  00   00
             149  75   -
```

ORIGINAL PAGE IS
OF POOR QUALITY

```
150  04   4
151  54   )
152  55   ÷
153  43  RCL
154  04   04
155  54   )
156  65   ×
157  53   (
158  43  RCL
159  05   05
160  75   -
161  43  RCL
162  04   04
163  39  COS
164  54   )
165  95   =
166  42  STO    am
167  10   10
-------------------
168  53   (
169  04   4
170  65   ×
171  53   (
172  43  RCL
173  00   00
174  75   -
175  04   4
176  54   )
177  33  X²
178  85   +
179  01   1
180  54   )
181  65   ×
182  43  RCL
183  05   05
184  75   -
185  53   (
186  02   2
187  55   ÷
188  43  RCL
189  04   04
190  33  X²
191  54   )
192  65   ×
193  53   (
194  43  RCL
195  05   05
196  75   -
197  43  RCL
198  04   04
199  39  COS
200  54   )
201  95   =
202  42  STO
203  11   11    bm
```

```
204  65   ×
205  43  RCL
206  01   01
207  55   ÷
208  04   4
209  09   9
210  95   =
211  94  +/-
212  42  STO
213  15   15
214  43  RCL
215  05   05
216  85   +
217  53   (
218  43  RCL
219  01   01
220  65   ×
221  43  RCL
222  10   10
223  55   ÷
224  04   4
225  09   9
226  54   )
227  95   =
228  42  STO
229  14   14
230  32  X:T
231  43  RCL
232  15   15
233  22  INV
234  37  P/R
235  42  STO
236  17   17
237  32  X:T
238  42  STO
239  16   16
240  43  RCL
241  00   00
242  85   +
243  02   2
244  09   9
245  95   =
246  42  STO
247  07   07
248  43  RCL
249  00   00
250  85   +
251  03   3
252  06   6
253  95   =
254  42  STO
255  08   08
256  73  RC*
257  07   07
```

```
258  65   ×
259  43  RCL
260  16   16
261  95   =
262  42  STO
263  18   18
264  73  RC*
265  08   08
266  85   +
267  43  RCL
268  17   17
269  85   +
270  53   (
271  02   2
272  65   ×
273  43  RCL
274  04   04
275  65   ×
276  53   (
277  43  RCL
278  00   00
279  75   -
280  04   4
281  54   )
282  54   )
283  95   =
284  42  STO
285  19   19
286  32  X:T
287  43  RCL
288  18   18
289  32  X:T
290  37  P/R
291  44  SUM
292  21   21
293  32  X:T
294  44  SUM
295  20   20
296  97  DSZ   m=m-1
297  00   00          Do loop: return to label D
298  14   D
-------------------
299  43  RCL
300  20   20
301  32  X:T
302  43  RCL
303  21   21
304  22  INV
305  37  P/R
306  42  STO
307  23   23
308  32  X:T
309  42  STO
310  22   22
```

```
311   65   ×
312   43   RCL
313   03    03
314   39   COS
315   95   =
316   42   STO
317   25    25
318   43   RCL
319   03    03
320   65   ×
321   05   5
322   07   7
323   93   .
324   03   3
325   95   =
326   99   PRT
327   43   RCL      |E(θ)|        [Power Normalized to 0 dB.]
328   25    25
329   55   ÷
330   53   (        (
331   43   RCL      I1
332   30    30
333   85   +        +
334   43   RCL      I2
335   31    31
336   85   +        +
337   43   RCL      I3
338   32    32
339   85   +        +
340   43   RCL      I4
341   33    33
342   85   +        +
343   43   RCL      I5
344   34    34
345   85   +        +
346   43   RCL      I6
347   35    35
348   85   +        +
349   43   RCL      I7
350   36    36
351   54   )        )
352   95   =
353   28   LOG
354   65   ×
355   02   2
356   00   0
357   95   =
358   99   PRT
359   43   RCL      φ             [φ: Phase angle of E(θ) (deg.)]
360   23    23
361   65   ×
362   05   5
363   07   7
364   93   .
365   03   3
366   95   =
367   99   PRT
368   98   ADV
369   43   RCL                    [Incr. θ by .05° and return to LBL C]
370   03    03
371   65   ×
372   05   5
373   07   7
374   93   .
375   02   2
376   09   9
377   05   5
378   07   7
379   08   8
380   95   =
381   85   +
382   93   .
383   00   0
384   05   5
385   95   =
386   61   GTO
387   13   C
388   76   LBL                    [SUBROUTINE SET STORAGE REGISTERS 14-21 TO 0.]
389   88   DMS
390   00   0
391   42   STO
392   14    14
393   00   0
394   42   STO
395   15    15
396   00   0
397   42   STO
398   16    16
399   00   0
400   42   STO
401   17    17
402   00   0
403   42   STO
404   18    18
405   00   0
406   42   STO
407   19    19
408   00   0
409   42   STO
410   20    20
411   00   0
412   42   STO
413   21    21
414   92   RTN
```

End of program

DATA

$\theta = +4.0^\circ$

Angle	Power (dB)	Phase (degrees)
-4.000	-24.643	11.862
-3.950	-23.149	11.243
-3.900	-21.935	10.860
-3.850	-20.936	10.631
-3.800	-20.110	10.510
-3.750	-19.429	10.471
-3.700	-18.875	10.498
-3.650	-18.434	10.584
-3.600	-18.096	10.723
-3.550	-17.855	10.915
-3.500	-17.708	11.159
-3.450	-17.652	11.462
-3.400	-17.687	11.828
-3.350	-17.815	12.267
-3.300	-18.040	12.795
-3.250	-18.368	13.430
-3.200	-18.806	14.201
-3.150	-19.368	15.148
-3.100	-20.070	16.333
-3.050	-20.936	17.849
-3.000	-21.998	19.850
-2.950	-23.304	22.600
-2.900	-24.923	26.594
-2.850	-26.952	32.845
-2.800	-29.483	43.650
-2.750	-32.311	64.204
-2.700	-33.726	99.239
-2.650	-31.930	132.435
-2.600	-29.125	151.060
-2.550	-26.710	161.001
-2.500	-24.795	166.914
-2.450	-23.284	170.816
-2.400	-22.086	173.613
-2.350	-21.142	175.759
-2.300	-20.410	177.503
-2.250	-19.865	178.997

-2.200
-19.491
180.345

-2.150
-19.281
181.624

-2.100
-19.236
182.902

-2.050
-19.363
184.251

-2.000
-19.679
185.756

-1.950
-20.212
187.542

-1.900
-21.007
189.809

-1.850
-22.140
192.921

-1.800
-23.732
197.640

-1.750
-25.978
205.825

-1.700
-29.062
222.868

-1.650
-31.623
261.609

-1.600
-29.197
-53.384

-1.550
-25.016
-31.851

-1.500
-21.604
-22.102

-1.450
-18.901
-16.812

-1.400
-16.689
-13.525

-1.350
-14.823
-11.287

-1.300
-13.211
-9.664

-1.250
-11.796
-8.431

-1.200
-10.539
-7.461

-1.150
-9.411
-6.677

-1.100
-8.393
-6.031

-1.050
-7.469
-5.488

-1.000
-6.627
-5.026

-0.950
-5.858
-4.629

-0.900
-5.155
-4.284

-0.850
-4.512
-3.981

-0.800
-3.924
-3.715

-0.750
-3.388
-3.478

-0.700
-2.899
-3.268

-0.650
-2.454
-3.081

-0.600
-2.053
-2.913

-0.550
-1.692
-2.762

-0.500
-1.369
-2.628

-0.450
-1.085
-2.507

-0.400
-0.836
-2.399

-0.350
-0.623
-2.302

-0.300
-0.444
-2.216

-0.250	0.400	1.050
-0.299	-1.466	-10.744
-2.140	-1.916	-4.241
-0.200	0.450	1.100
-0.187	-1.811	-12.223
-2.074	-1.959	-4.859
-0.150	0.500	1.150
-0.108	-2.199	-13.961
-2.016	-2.014	-5.711
-0.100	0.550	1.200
-0.062	-2.632	-16.063
-1.967	-2.081	-6.970
-0.050	0.600	1.250
-0.049	-3.115	-18.719
-1.926	-2.162	-9.023
0.000	0.650	1.300
-0.069	-3.651	-22.335
-1.892	-2.260	-12.994
0.050	0.700	1.350
-0.122	-4.244	-27.992
-1.867	-2.376	-23.865
0.100	0.750	1.400
-0.208	-4.900	-36.481
-1.850	-2.514	-87.848
0.150	0.800	1.450
-0.328	-5.627	-28.935
-1.840	-2.678	202.672
0.200	0.850	1.500
-0.482	-6.433	-23.705
-1.838	-2.876	191.037
0.250	0.900	1.550
-0.672	-7.330	-20.610
-1.844	-3.115	186.862
0.300	0.950	1.600
-0.899	-8.332	-18.509
-1.859	-3.408	184.688
0.350	1.000	1.650
-1.163	-9.461	-16.982
-1.883	-3.774	183.318

1.700	-15.832	182.346	2.350	-14.883	174.402	3.000	-26.269	45.290
1.750	-14.953	181.592	2.400	-15.543	173.324	3.050	-24.498	35.940
1.800	-14.284	180.967	2.450	-16.324	172.016	3.100	-23.025	29.968
1.850	-13.783	180.418	2.500	-17.241	170.392	3.150	-21.835	25.926
1.900	-13.423	179.913	2.550	-18.317	168.318	3.200	-20.882	23.056
1.950	-13.187	179.429	2.600	-19.579	165.580	3.250	-20.127	20.940
2.000	-13.061	178.949	2.650	-21.066	161.814	3.300	-19.542	19.338
2.050	-13.037	178.457	2.700	-22.821	156.369	3.350	-19.103	18.102
2.100	-13.110	177.941	2.750	-24.875	148.013	3.400	-18.795	17.138
2.150	-13.276	177.385	2.800	-27.147	134.456	3.450	-18.606	16.386
2.200	-13.534	176.775	2.850	-29.103	112.678	3.500	-18.530	15.803
2.250	-13.885	176.092	2.900	-29.533	84.564	3.550	-18.562	15.365
2.300	-14.333	175.311	2.950	-28.188	60.620	3.600	-18.700	15.053

3.650
-18.945
14.858

3.700
-19.302
14.779

3.750
-19.776
14.822

3.800
-20.380
15.001

3.850
-21.128
15.344

3.900
-22.046
15.899